Conference paper

Bo Zhang, Tomas Mikysek, Veronika Cicmancova, Stanislav Slang, Roman Svoboda, Petr Kutalek and Tomas Wagner*

2D $GeSe_2$ amorphous monolayer

https://doi.org/10.1515/pac-2019-0501

Abstract: In this paper, $GeSe_2$ thin film and glass ingot were prepared in a layered structure. Subsequently, the 2D amorphous monolayers were achieved from layered thin film and layered glass ingot. The thicknesses of monolayers from thin film range from 1.5 nm to 5 nm. And the thickness of monolayer from glass ingot is 7 μm. The fast cooling of material results in the formation of self-assembled monolayers. In the case of thin film, layers are connected with "bridge". After doping of Ag, the precipitation of nano particles exfoliates the adjacent monolayers which can be further dispersed by etching of Ag particles. In the case of glass ingot, the composition changes at 1 % between adjacent monolayers, according to EDX (energy-dispersive X-ray spectroscopy) spectra. And the glass 2D monolayer can be mechanically peeled off from the glass ingot.

Keywords: 2D amorphous chalcogenide; SSC-2018.

Introduction

The layered structure in chalcogenide glass has been widely studied. Firstly, Phillips [1] suggests a distorted layer model for glass, where deformed covalent layers are present with interlayer distance of ~0.6 nm. Secondly, the pressure dependence of glass GeS_2 is similar as layered crystal $GeSe_2$, which proves the existence of van der Waals interactions [2]. Furthermore, Shimakawa et al. [3] assumes the existence of interlayer distortion inside Ge–Se thin film. The orientation of interlayers is randomly arranged within internal space. Specifically, the bandgap illumination can indeed cause the volume change of chalcogenide thin film [4]. The photo-induced volume expansion in As_2S_3 films is even higher than 5 % [5]. Except of the illumination, annealing below glass transition temperature would also change the volume of chalcogenide thin film. For example, the volume of As_2S_3 changes by 2 %, after annealing at 160 °C [6].

Article note: A collection of invited papers based on presentations at the 13th International Conference on Solid State Chemistry (SSC-2018), Pardubice, Czech Republic, September 16–21, 2018.

***Corresponding author: Tomas Wagner,** Department of General and Inorganic Chemistry, Faculty of Chemical Technology, University of Pardubice, Studentska 573, 532 10 Pardubice, Czech Republic; and Center of Materials and Nanotechnologies, Faculty of Chemical Technology, University of Pardubice, Nam. Cs. Legii 565, 530 02 Pardubice, Czech Republic, e-mail: tomas.wagner@upce.cz

Bo Zhang: Department of General and Inorganic Chemistry, Faculty of Chemical Technology, University of Pardubice, Studentska 573, 532 10 Pardubice, Czech Republic

Tomas Mikysek: Department of Analytical Chemistry, Faculty of Chemical Technology, University of Pardubice, Studentska 573, 532 10 Pardubice, Czech Republic

Veronika Cicmancova and Stanislav Slang: Center of Materials and Nanotechnologies, Faculty of Chemical Technology, University of Pardubice, Nam. Cs. Legii 565, 530 02 Pardubice, Czech Republic. https://orcid.org/0000-0001-7760-2964 (S. Slang)

Roman Svoboda: Department of Physical Chemistry, Faculty of Chemical Technology, University of Pardubice, Studentska 573, 532 10 Pardubice, Czech Republic

Petr Kutalek: Joint Laboratory of Solid State Chemistry, University of Pardubice, Studentska 84, 532 10 Pardubice, Czech Republic

The dissolution of chalcogenide films is explored by Chern et al. [7]. They investigated the dissolution of arsenic sulfide in n-propylamine and n-butylamine. The solvent breaks up the layered structure into the small flat clusters. The etching process starts from the defect sites between layers [8]. Besides amine solvents, the chalcogenide glass is also unstable in alkaline water solutions, where the dissolution mechanism can be explained by the nucleophilic substitution [9].

The other important properties of chalcogenide thin film are photo-doping of metals and their photo-surface deposition [10]. The photo-doped Ag concentration profile is proved to be "step-like" in the chalcogenide thin films [11]. When the Ag^+ ions reach the surface of thin film, those can precipitate on the surface of chalcogenide thin film, (i.e. "photo surface deposition" [12]). The photo-doping and photo-surface deposition are closely related due to the structure and composition of amorphous chalcogenides [10].

The chalcogenide material can be made in 2D structure. After Novoselov et al. prepared the single layer graphene, various different 2D crystalline materials have been found as well [13, 14]. 2D-TMDs (Transition metal dichalcogenide), including MoS_2, $MoSe_2$, are well studied [15]. The preparation methods of 2D crystalline material ranges from mechanical liquid exfoliator to vapor based CVD synthesis [16, 17]. The emerging application of 2D crystalline material comprises from transistors to sensors [18, 19]. Except for TMDs, post-transition-metal dichalcogenides are also an important group of materials which can be the generally described by the formula MX (M = Ga, In and X = S, Se, Te). These compounds also exhibit a layered two-dimensional structure [20]. The attractive properties of these compounds give various applications [21, 22].

As discussed above, chalcogenide compounds are closely related to multilayer structure. However, the layered thin films prepared by thermal evaporation are rarely discussed in publications. In this letter, thermally deposited Ag-doped $GeSe_2$ films were chemically etched. The etching led to delamination and exfoliation of the Ag-doped films into monolayers. Such structural features can be also found on the surface of a water cooled bulk glass ingot. The possible mechanism is further analyzed by the computer simulation.

Experimental section

$GeSe_2$ glass was synthesized using the melt-quenching technique from high purity elements of Ge (5N) and Se (4N5). An ampoule loaded with raw elements was sealed at a pressure of ~10^3 Pa and heated in a rocking furnace at 900 °C for 12 h. Then the ampule was cooled in water (15 °C). The thin film was prepared from the powder of glass ingot by simple thermal evaporation at the pressure of ~10^{-4} Pa. The evaporation speed is controlled at ~5 nm/s. The substrate is kept at ambient temperature before evaporation. The details of samples are listed in the Table 1.

Two different samples are shown in Table 1, where Ag doped samples are labelled as No. 1. In case of the sample No. 1, the Ag was evaporated onto the $GeSe_2$ thin film. During deposition, the Ag can directly diffuse into the chalcogenide thin film. The driving force for Ag diffusion might come from the emitted light and transferred heat from the boat. After deposition, there is no metallic layer on the chalcogenide thin film and the surface is insulating. In the sample No. 2, the pure $GeSe_2$ chalcogenide layer was evaporated. After deposition, the 6.3 g/l $FeCl_3$ acetone solution was dropped onto the surface of Ag doped $GeSe_2$ thin film. Ag and $FeCl_3$ reacted immediately. Meanwhile, the remaining solution on the surface of thin film contains Ge–Se flakes. Afterwards, solution with flakes was transferred onto the W layer (for SEM and AFM observation) and onto Au TEM grid (for STEM). After drying off the acetone, the Ge–Se flakes were present on the W layer and Au TEM grid.

Table 1: The details of samples.

Number	The evaporation sequence	Final sample
1	$GeSe_2$ (500 nm)–Ag (15 nm)	Glass substrate/$AgGeSe_2$
2	$GeSe_2$ (2.5 μm)	Glass substrate/$GeSe_2$

The thicknesses of Ge–Se flakes were determined via AFM (Atomic Force Microscope) images (AFM Solver Pro M, NT-MDT in semi-contact mode). The surface and cross sectional morphology was studied from SEM (scanning electron microscope) images (JEOL 7500 at 5 kV acceleration voltage). The cross sectional view of thin film and glass ingot were obtained by mechanical cleavage. All the samples for SEM observation were covered with a layer of carbon film (~5 nm). The flake morphology and composition were characterized by STEM (scanning transmission electron microscope) images and EDX (energy-dispersive X-ray spectroscopy) measurements (LYRA3 GMH, TESCAN at 30 kV acceleration voltage). Measurements of digital holographic microscope (DHM) were realized to study the steps of the etched thin film (DHMR1000, LyncéeTec, Switzerland, operating at 785 nm in reflection configuration). Optical images were taken from BX 51, Olympus.

Results and discussion

According to the literature, the etching of $AgGeSe_2$ is rather difficult. Chemicals, for instance alkaline cyanate, were used as an etchant [23]. Due to high Ag concentration in $GeSe_2$ film, silver precipitates inside the film and exfoliates the film into monolayers. The Ag particles, which precipitated between chalcogenide layer and substrate, often result in the stress induced fissure throughout the chalcogenide film. Generally, the chemical etching of precipitated Ag in Ag doped $GeSe_2$ film leads to delamination and exfoliation of chalcogenide monolayers. In this work, $FeCl_3$ acetone solution was used as etchant. Acetone plays an important role in etchant: Firstly, $FeCl_3$ can be dissolved in acetone at room temperature. Secondly, acetone has low surface tension. Therefore, it could flow into the gap between monolayers. Thirdly, the intercalation of acetone molecules would further separate the adjacent monolayers. Based on the three reasons, the cracks or voids in chalcogenide film are very important to facilitate the etching process. Then, the $FeCl_3$/acetone etchant does not etch the thin film but the Ag particles inside the thin film. After the silver phase between monolayers is etched away, the thin film is exfoliated. The suggested reaction mechanism of silver dissolution can be described as [24, 25]:

$$FeCl_3 + Ag \xrightarrow{\text{reaction}} FeCl_2 + AgCl$$

An observation of the etched $AgGeSe_2$ thin film and its micro/nano structure are presented in Fig. 1. The sample was evaporated in two steps. Firstly $GeSe_2$ was deposited (500 nm) and then, another deposition of the 15 nm Ag was followed. During the deposition of the Ag layer, silver atoms were quantitatively dissolved into the $GeSe_2$ thin film under the emitted light from heated evaporation boat simultaneously. Figure 1a shows the $AgGeSe_2$ film after $FeCl_3$ solution etching, where three distinct monolayers can be recognised. The order from the top to the bottom is marked as 1–3. During etching process, the $FeCl_3$ solution etches Ag particle at the surface or between monolayers. Therefore, the monolayers are peeled off. On the 3rd layer, a black dot and white boundary pattern are clearly identified. It is the result of the growth of Ag particles at the interface between chalcogenide layer and glass substrate, where the bulk silver particles cause the regional delamination from glass substrate. The Ag doped chalcogenide film consists of "monolayers" shown in Fig. 1a. The 2D monolayers are paralleled in stack. Therefore, the cross section observation is necessary for further identification of the thin film morphology. Figure 1b gives the cross sectional view of thin film, where the layered structure can be observed at the red arrow. The morphology of dark and bright stripes is shown on the side of cross section, which represents different monolayers. Figure 1c gives closer view of monolayers, where a structure "2D monolayer-Ag particles-2D monolayer" is identified. The surface Ag particles (marked by red arrow) separate underneath monolayer from the top monolayer (marked by yellow arrow). In summary, Fig. 1d illustrates the thin film structure before and after etching. In the first step, the precipitated Ag particle creates the internal stress, and such stress induces the crack on the monolayers. In the second step, the acetone/$FeCl_3$ flows into the cracks and further exfoliates the thin film.

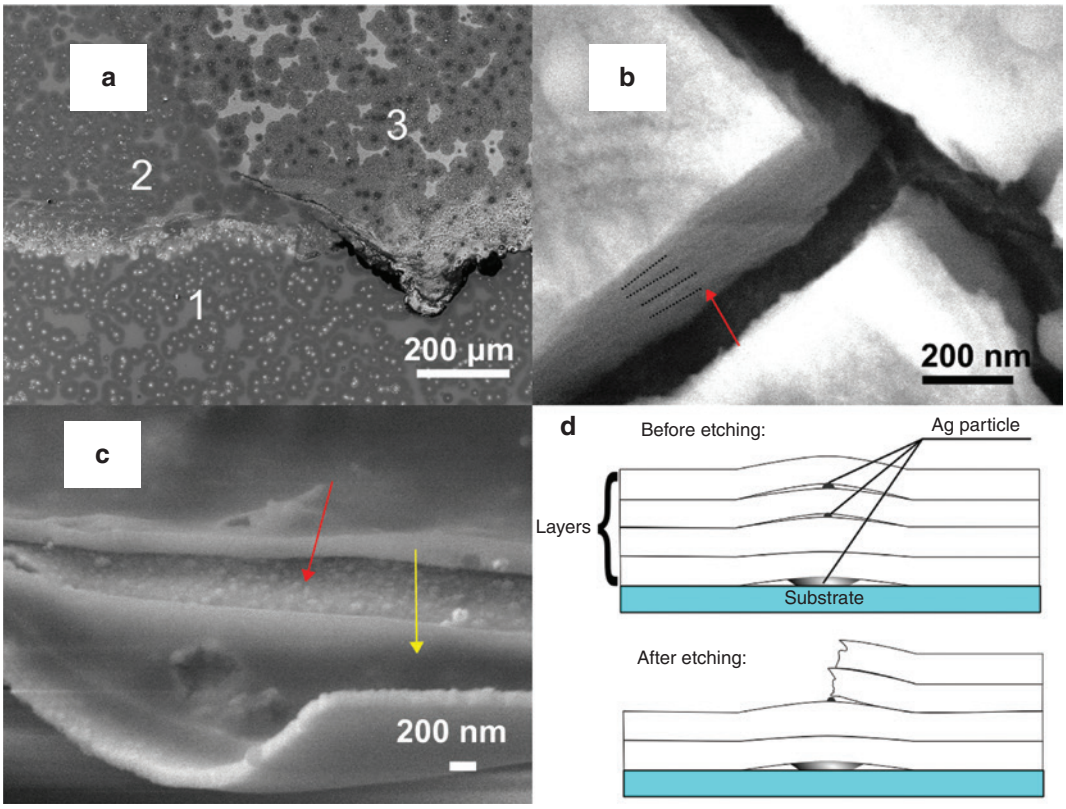

Fig. 1: (a) The etched Ag doped $GeSe_2$ thin film. The monolayer sequence from the top to the bottom is marked from 1 to 3. (b) SEM image of the cross section along the film after etching. The red arrow points out to the edge of the film where monolayers are observable. The black dash line marks the position of black strips. (c) The nano structure of $AgGeSe_2$ delaminated monolayers. The yellow arrow points at the top monolayer. And the red arrow points at the monolayer underneath. (d) The illustration of thin film structure before and after etching. The black dots represent Ag particles.

As characterized in Fig. 1a and b, Ag doped chalcogenide thin film comprises of the stacked 2D monolayers. The thickness of stacked 2D monolayers is studied via digital holographic microscopy [26]. The profiles were measured in Fig. 2a along the line *a* and line *b*. From the Fig. 2b, three different steps are marked with step 1, step 2 and step 3, along profile of the line *a*. The average thickness of 2D monolayers (step 1–3) is approx. 50 nm. From the Fig. 2c, the thickness of other monolayer (step 4) is approx. 60 nm. Figure 2d shows the detail of the dashed circle in Fig. 2c, which includes two 2D monolayers, marked layer 1 and layer 2. The thickness of layer 1 and 2 is 20 nm and 10 nm, respectively. In summary, the thickness of 2D monolayer varies from 60 nm to 10 nm, according to the study of etched thin film.

For further understanding of ongoing lamination process, it is important to acquire the 2D monolayer from etching. The $FeCl_3$ acetone solution breaks the thin film into flakes. The flakes were then transferred onto a gold TEM grid and a substrate which was covered by sputtered W thin film. After drying, the gold TEM grid with attached flakes was analyzed by STEM, and the W covered thin film with flakes was analyzed by SEM and AFM (the W thin film is inert to $FeCl_3$ acetone solution). Figure 3a shows the STEM images of flakes placed on the standard Au TEM grid, where two kinds of particles can be recognized: the semi-transparent type and black opacity type. Black opacity particle (pointed by red arrow) attributes to remaining Ag particle and the transparent square shape particle (pointed by yellow arrow) is assumed to be the remaining layers. The background shows the inhomogeneous white and gray contrast, which implies the thickness or composition variation throughout the flakes. Figure 3b shows the SEM image of $AgGeSe_2$ flakes on W thin film. Two different types of flakes can be seen: one is referred to as “thick flakes” (pointed by the red arrow); and another is the “thin flakes” (which is remaining grey islands deposited on

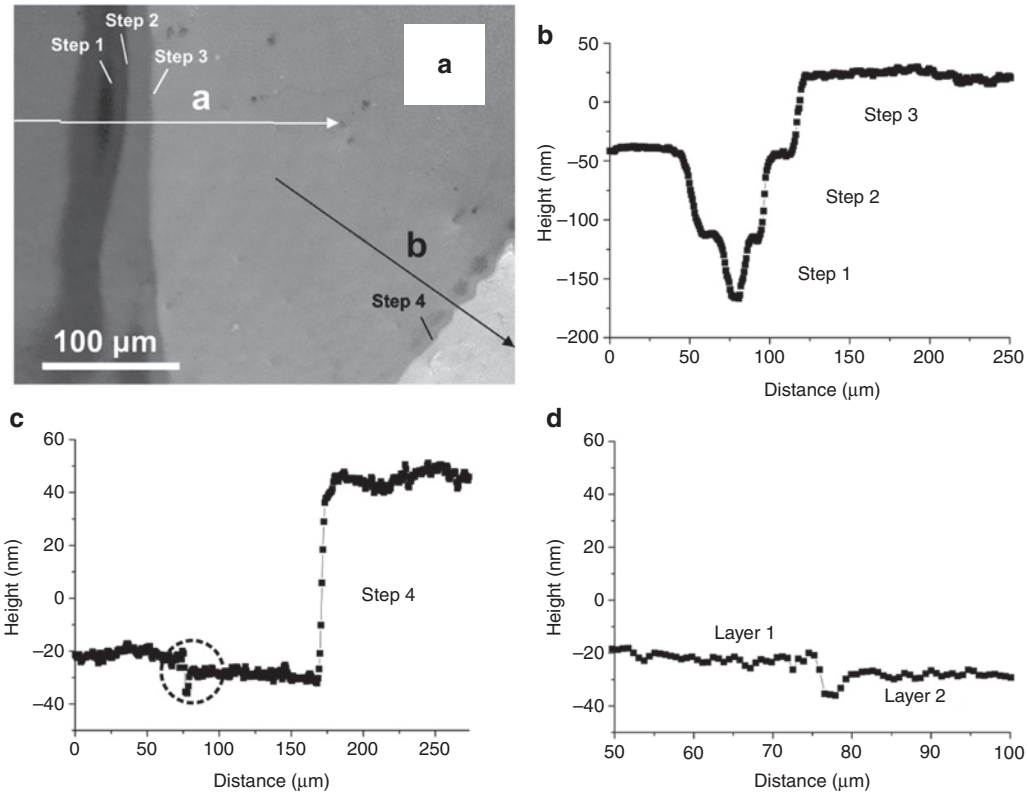

Fig. 2: 2D Digital Holographic microscopy image of etched Ag doped $GeSe_2$ thin film. (a) Optical image of etched thin film and profiles (a and b) are presented. (b) The profile along the direction a. individual steps 1–3 are labeled. (c) The profile along direction of b. Step 4 is labeled. (d) The enlarged area in circle of Fig. 2c.

the W film). The thick flake is possibly in corresponding with the steps in Fig. 2b; the thin flake is in corresponding with monolayers in Fig. 2d. Therefore, the thickness of thick flakes with gap can be deduced from the steps in Fig. 2b, where the thickness is 50–60 nm. Obviously, the morphology of thin flake is more interesting to study. Figure 3c and d shows the AFM topography and phase image of thin flakes deposited on the W film. In Fig. 3d, more flakes can be found on the W film in comparison with Fig. 3c. However, due to its small size and thickness, it is almost impossible to identify them from the topography image in Fig. 3c. Two profiles are taken from the dashed line positions in Fig. 3c and d. The left flake is composed from two monolayers, which are marked with yellow and green arrows. In more detail, the thickness of top monolayer is approx. 1.5 nm and thickness of bottom monolayer is approx. 5 nm, as described in Fig. 3e and f. In Fig. 3c, large peaks on the right flake (pointed by the blue arrow) can be assumed as a kind of deformation and the thickness of the flake on its edge is approx. 2 nm (as shown in Fig. 3g and h). As discussed above, the thinnest monolayers range from 1.5 to 2 nm. The AFM study provides fruitful information of flakes. However, there are still questions needed to be answered regarding with the structure model of the film.

As discussed above, after etching, some monolayers are not peeled off and it could be observed directly under SEM, as shown in Fig. 4a. We propose a structure model for Ag doped $GeSe_2$ thin films based on presence of bridges that connect the distinct 2D monolayers. The proposed bridges also serve as channels for the migration of Ag^+ ions. As shown in Fig. 4b, the Ag ions are diffusing from the bottom to the top via the "bridges". If the bridge is broken, the Ag^+ ions are not able to go across the gap. In consequence of that, the concentration of Ag^+ ions is increased continuously at the broken bridge edge and the Ag particles are formed there. The thin layer suffers from the internal expansion of the particle growth. Meanwhile, some intact bridges are still present in material and connect monolayers.

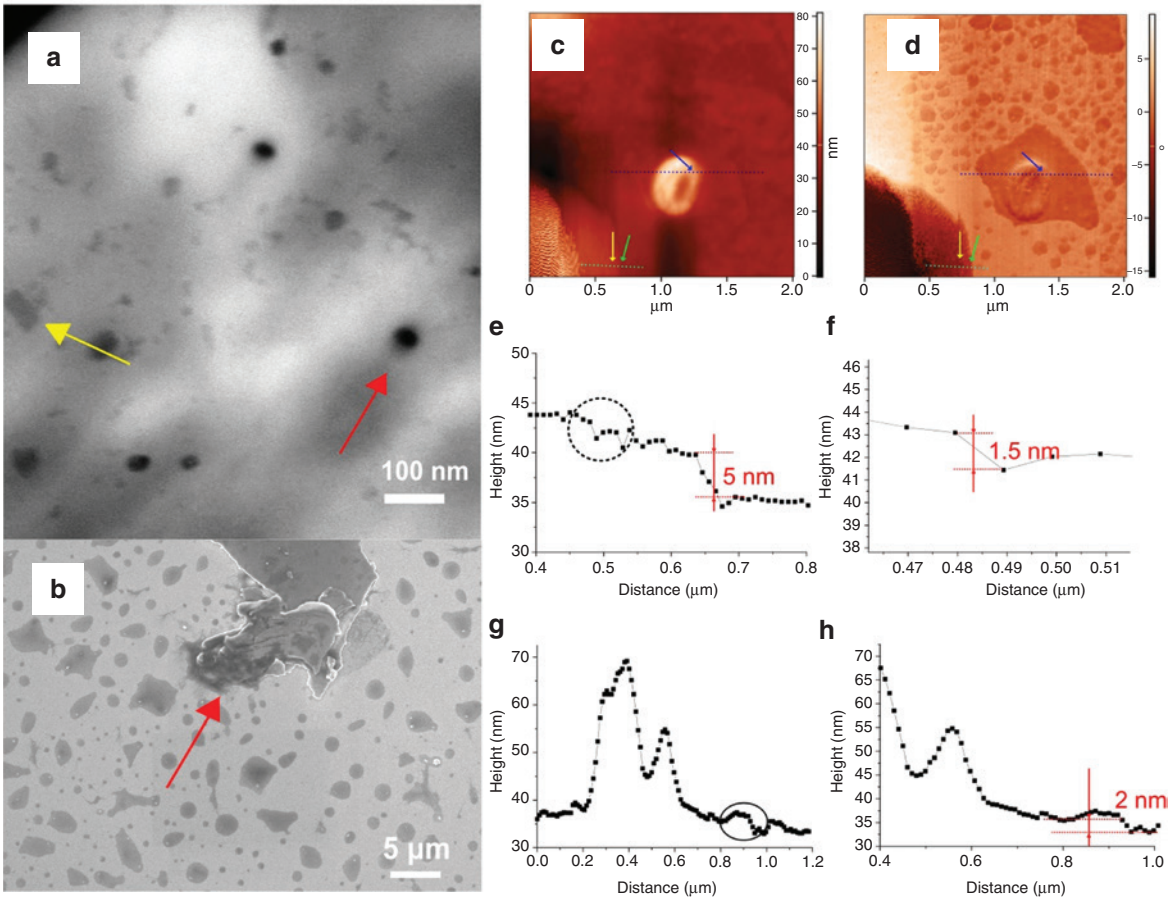

Fig. 3: (a) The STEM image of $AgGeSe_2$ flake. The yellow arrow points at the transparent square shape particle and red arrow points at the opacity Ag particle. (b) The SEM image of $AgGeSe_2$ flakes deposited onto W film. The red arrow points at the thick flakes. (c)–(h) The AFM topography of $AgGeSe_2$ flakes deposited onto W film. (c) The topography mapping of $AgGeSe_2$ flakes. (d) The phase image of $AgGeSe_2$ flakes. (e)–(f) The profiles at the dashed line position, pointed by yellow and green arrows in (c) and (d). (g)–(h) The profile at the dashed line position pointed by blue arrow in (c) and (d).

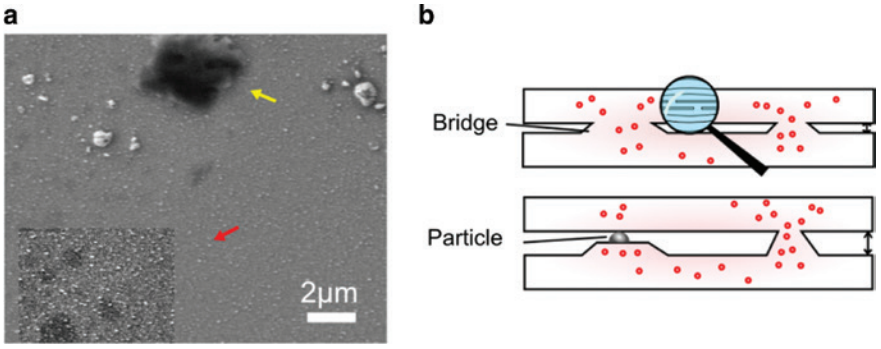

Fig. 4: (a) The SEM image of the etched Ag doped $GeSe_2$ with remaining monolayer. The yellow arrow points at the thick remaining monolayer and red arrow points at thin remaining monolayer with an increased contrast. (b) The illustrative picture of bridge-monolayer structure. The red spots represent Ag ions and black spots represent for Ag particle.

The origin of the layered structure is still unclear. As the thin film is evaporated from the powder of glass ingot, similar study is preformed to Ge–Se glass ingot. The glass ingot of $GeSe_2$ was prepared from melt and cooled in water at 15 °C. After that, the piece of glass ingot was studied under optical microscope. Figure 5a

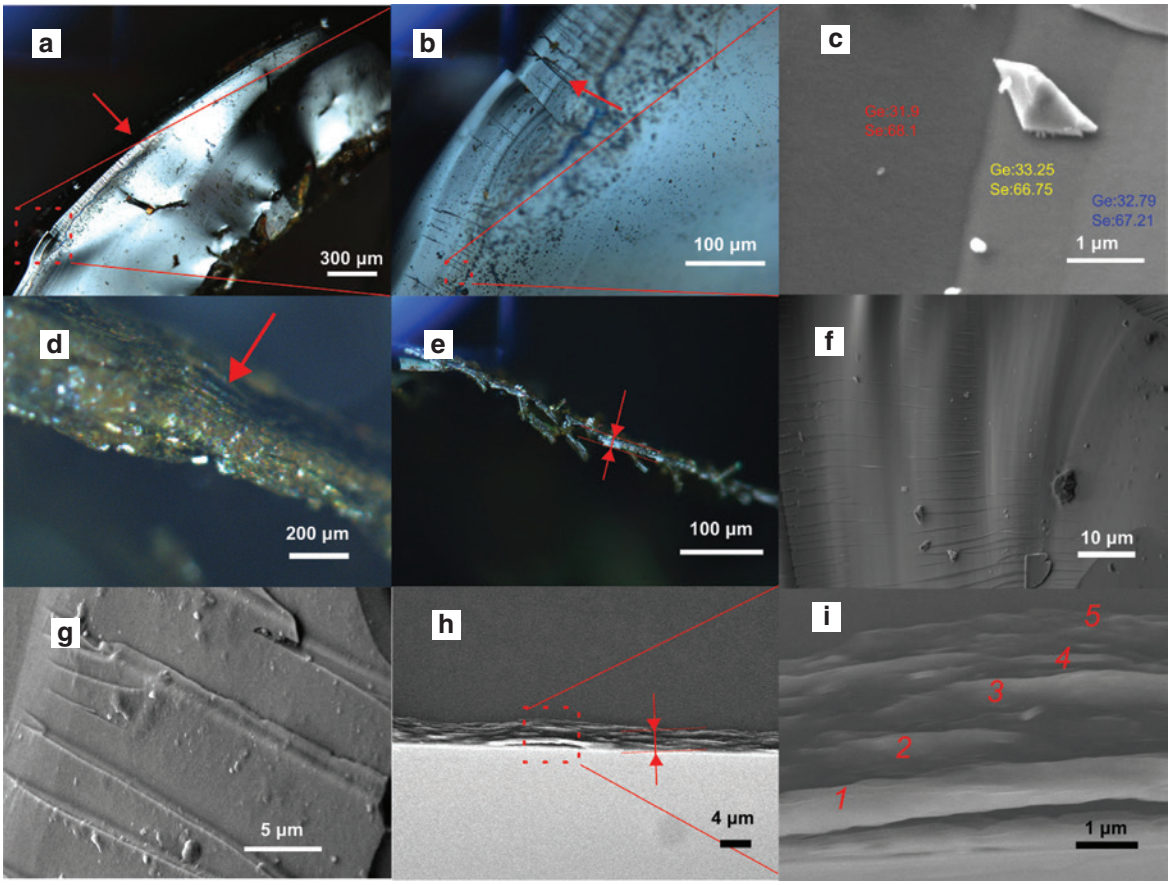

Fig. 5: (a) The optical image of cross-section in $GeSe_2$ glass ingot. The red arrow points at the monolayers. (b) The enlarged optical image from (a). (c) The SEM image of enlarged monolayer in (b) with composition measured by EDX. (d) The optical image of $GeSe_2$ ingot from the side view. The steps of monolayers are pointed out by the red arrow. (e) The optical image of $GeSe_2$ glass monolayer. (f) The cracks throughout the monolayers. (g) High magnification SEM images of cracks. (h) The cross sectional view of as-deposited $GeSe_2$ thin film. (i) Enlarged image from (h). The number of monolayers is marked from 1 to 5.

shows the cross section of $GeSe_2$ glass ingot in vicinity to the wall of ampule. Two distinct layers are pointed out by the red arrow. The layer closer to the wall of ampule is magnified in Fig. 5b. More rings appear at surface of glass. Further analysis by SEM and EDX in Fig. 5c shows the tiny change of Ge composition at approx. 1 at.% between adjacent monolayers. From the tilted glass view (Fig. 5d), the step-like morphology is pointed by the red arrow. The $GeSe_2$ glass monolayer is 7 μm thick, where is peeled mechanically from glass inogt as it is shown in Fig. 5e. The existence of internal stress also induces multiple cracks throughout the layers, shown in Fig. 5f and g.

Similarly, the layered structure should be also formed in the Ge–Se thin film during thermal evaporation. In the other words, Ag doping and precipitation are the way to exfoliate the Ge–Se monolayers, rather than reason of layers formation. Figure 5h shows a $GeSe_2$ film (approx. 2.5 μm) deposited by thermal evaporation. The similarity between glass ingot (5b) and thin film (5h) is clearly observed. The thin film consists of a layered structure. Moreover, internal stress is existed between monolayers. In the dash square, the thin film is detached with the substrate. Figure 5i gives a high magnification image of thin film where at least five monolayers are in staking.

The computer simulation in software Energy 2D [27] gives a general overview of process when the melt cools down into glass ingot as shown in Fig. 6a. The initial solid layer (500 μm) is assumed to be formed at the beginning of cooling. The continuous growth of solid layers heavily relies on its temperature. “a”, “b” and

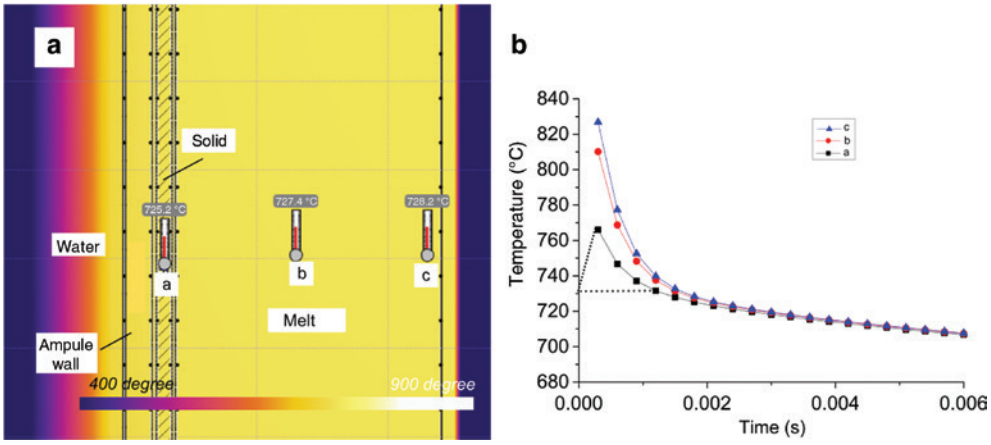

Fig. 6: (a) The computer simulated temperature distribution of glass ingot after 0.002 s cooling, where the thickness of ampule wall, solid is 1 mm and 500 μm, respectively. (b) The temperature variation of thermometers marked from (a).

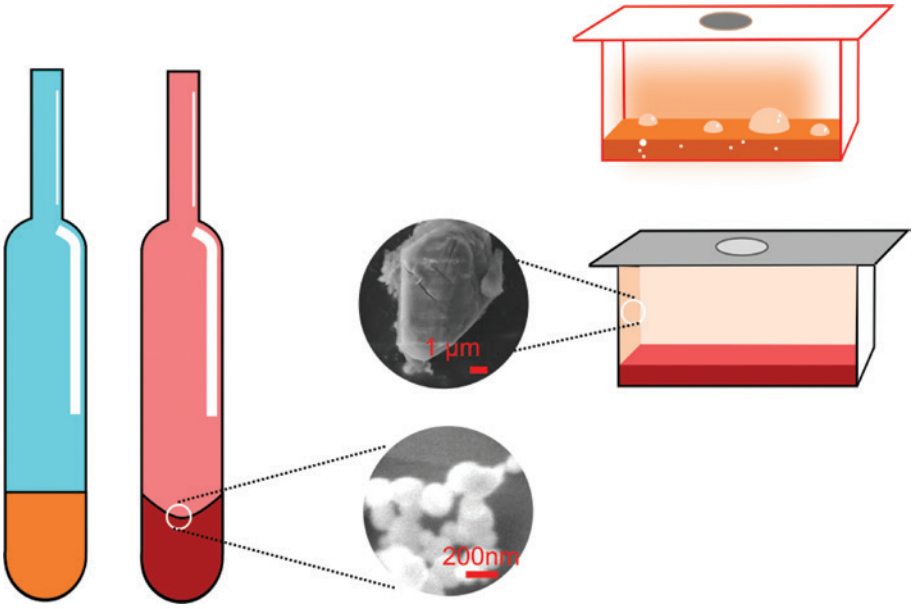

Fig. 7: The SEM images of particles formed on the hot wall of ampule (left figure) and evaporation boat (right figure).

"c" represent three thermometers, where the measured temperature with time is shown in Fig. 6b. The initial condition of the temperatures in water, ampule wall, solid layer and melt is 15 °C, 681 °C, 731 °C and 900 °C, respectively. The temperature of solid phase is obtained from phase diagram [28]. In the other words, solid $GeSe_2$ is formed at 731 °C. The temperature in ampule wall is calculated in the balanced state between water and solid phase.

After being cooled (the time starts to be counted after the formation of initial solid layer), temperature of solid layer increased from 731 °C to 795 °C. When the solid layer cools down back to 731 °C, the solidification from the melt continuously forms 2nd layer. Until second layer forms completely, the temperature of 2nd layer will increase again and next cycle begins. The repeatable cycles are marked with dashed line in Fig. 6b. The figure also shows the trends between thermometer c and b which similar variations prove the uniform temperature distribution in the interior of melt. In summary, the layer formation is attributed to interaction of "cold" and "heat" source.

Due to the high similarity of layers morphology between Ge–Se thin film and glass ingot, the layers formation in glass and thin film could have the same reason. However, there are still difficulties with the formation of layered thin film. It is assumed that the Ge–Se vapors should be condensed into a film in melt for a short interval. Then, the melt is cooled to solid layer. The condensation of the vapor on hot substrates gives possible evidence about melt existence, as shown in Fig. 7. For example, the vapor is condensed into nano particles on the hot ampule (left SEM image in Fig. 7) or micro particle on the hot wall of hot evaporation boat (right SEM image in Fig. 7). It manifests that the vapor could be condensed into liquid form for a short time period [29]. In summary, we know that the layer between glass and thin film is similar. However, the model with thin film is not simulated, due to its complexity for software. And more questions are still need to discuss in future.

Conclusions

In conclusion, layered amorphous material is fabricated. Due to the similarity of structures between thin film and glass ingot, the layered material is possibly formed due to fast cooling. Furthermore, we put forward a "bridge" model and the formation of 2D monolayers is also presented via computer simulation. In the case of thin film, layers are connected with "bridge". After doping of Ag, the precipitation of nano particles exfoliates the adjacent monolayers which can be further dispersed by etching of Ag particles. In the case of glass ingot, the composition changes at 1 % between adjacent monolayers, according to EDX spectra. And the glass 2D monolayer can be mechanically peeled off from the glass ingot.

In our amorphous 2D material, the preparation method and dimension of flakes are obviously different from classic 2D material [30]. Nevertheless, since we utilized standard sputtering and melt quenching methods to prepare the thin film and glass ingot, the layered structure formation should be a common physical phenomenon. Therefore, the simple preparation of 2D amorphous monolayer could make it possible for broad applications. At last, it can be also expected the conversion between amorphous 2D monolayer and crystal 2D monolayer in the future study.

Acknowledgements: The authors thank for financial support from the grant of the Ministry of Education, Youth and Sports of Czech Republic (Funder Id: http://dx.doi.org/10.13039/501100001823, grant LM2015082), the European Regional Development Fund-Project "Modernization and upgrade of the CEMNAT" (Funder Id: http://dx.doi.org/10.13039/501100008530, No. CZ.02.1.01/0.0/0.0/16_013/0001829), and the project of Czech Grant Agency (GA CR) Funder Id: http://dx.doi.org/10.13039/501100001824, 19-17997S.

References

[1] J. C. Phillips. *J. Non. Cryst. Solids* **43**, 37 (1981).
[2] K. Tanaka. *Solid State Commun.* **58**, 469 (1986).
[3] K. Shimakawa, N. Yoshida, A. Ganjoo, Y. Kuzukawa, J. Singh, *Philos. Mag. Lett.* **77**, 153 (1998).
[4] H. Hamanaka, K. Tanaka, A. Matsuda, S. Iizima. *Solid State Commun.* **19**, 499 (1976).
[5] H. Hisakuni, K. Tanaka. *Appl. Phys. Lett.* **65**, 2925 (1994).
[6] D. Y. Choi, A. Wade, S. Madden, R. Wang, D. Bulla, B. Luther-Davies. *Physics Procedia*. **48**, 196 (2013).
[7] G. C. Chern, I. Lauks, K. H. Norian. *Thin Solid Films* **123**, 289 (1985).
[8] G. C. Chern, I. Lauks. *J. Appl. Phys.* **54**, 2701 (1983).
[9] S. Mamedov. *Thin Solid Films* **226**, 215 (1993).
[10] M. Frumar, T. Wagner. *Curr. Opin. Solid State Mater. Sci.* **7**, 117 (2003).
[11] T. Wágner, A. Macková, V. Peřina, E. Rauhala, A. Seppälä, S. O. Kasap, M. Frumar, M. Vlček, M. Vlček. *J. Non Cryst. Solids* **299–302**, 1028 (2002).
[12] B. Zhang, M. Fraenkl, J. M. Macak, T. Wagner. *Mater. Lett.* **163**, 4 (2016).

[13] K. S. Novoselov, A. K. Geim, S. V. Morozov, D. Jiang, Y. Zhang, S. V. Dubonos, I. V. Grigorieva, A. A. Firsov. *Science* **306**, 666 (2004).
[14] C. Tan, X. Cao, X. J. Wu, Q. He, J. Yang, X. Zhang, J. Chen, W. Zhao, S. Han, G. H. Nam, M. Sindoro, H. Zhang. *Chem. Rev.* **117**, 6225 (2017).
[15] D. Voiry, A. Mohite, M. Chhowalla. *Chem. Soc. Rev.* **44**, 2702 (2015).
[16] V. Nicolosi, M. Chhowalla, M. G. Kanatzidis, M. S. Strano, J. N. Coleman. *Science* **340**, 1420 (2013).
[17] C. Tan, H. Zhang. *Nat. Commun.* **6** (2015). Article number: 7873.
[18] L. Li, Y. Yu, G. J. Ye, Q. Ge, X. Ou, H. Wu, D. Feng. *Nat. Nanotechnol.* **9**, 1 (2014).
[19] H. Li, Z. Yin, Q. He, H. Li, X. Huang, G. Lu, D. W. H. Fam, A. I. Y. Tok, Q. Zhang, H. Zhang. *Small* **8**, 63 (2012).
[20] J. Luxa, Y. Wang, Z. Sofer, M. Pumera. *Chem. – A Eur. J.* **22**, 18810 (2016).
[21] J. Kang, S. A. Wells, V. K. Sangwan, D. Lam, X. Liu, J. Luxa, Z. Sofer, M. C. Hersam. *Adv. Mater.* **30**, 1802990 (2018).
[22] P. Marvan, V. Mazánek, Z. Sofer. *Nanoscale* **11**, 4310 (2019).
[23] J. Orava, T. Wagner, M. Krbal, T. Kohoutek, M. Vlcek, P. Klapetek, M. Frumar. *J. Non Cryst. Solids* **354**, 533 (2008).
[24] Y. Aoshima, M. Miyazaki, K. Sato, Y. Akao, T. Satoru, K. Adachi. *Jpn. J. Appl. Phys.* **40**, 4166 (2001).
[25] T.-S. Choi, D. W. Hess. *ECS J. Solid State Sci. Technol.* **4**, N3084 (2014).
[26] P. Knotek, D. Arsova, E. Vateva, L. Tichý. *J. Optoelectron. Adv. Mater.* **11**, 391 (2009).
[27] C. Xie. *Phys. Teach.* **50**, 237 (2012).
[28] A. Laugier, G. Chaussemy, J. Fornazero. *J. Non Cryst. Solids* **23**, 419 (1977).
[29] J. A. Venables, G. D. T. Spiller, M. Hanbucken. *Rep. Prog. Phys.* **47**, 399 (1984).
[30] Y. Ye, Q. Guo, X. Liu, C. Liu, J. Wang, Y. Liu, J. Qiu. *Chem. Mater.* **29**, 8361 (2017).